Neutron and X-ray single-crystal study of the AlPdMn icosahedral phase

1992 J. Phys.: Condens. Matter 4 10149

(http://iopscience.iop.org/0953-8984/4/50/007)

J. Phys.: Condens. Matter 4 (1992) 10149–10168. Printed in the UK

Neutron and x-ray single-crystal study of the AlPdMn icosahedral phase

M Boudard†‡, M de Boissieu‡, C Janot†, G Heger§, C Beeli||§§, H-U Nissen||, H Vincent¶, R Ibberson††, M Audier‡ and J M Dubois‡‡

† Institut Laue–Langevin, BP 156, 38042 Grenoble Cédex 9, France
‡ LTPCM-ENSEEG, BP 75, 38402 St Martin d'Hères Cédex, France
§ Laboratoire Léon Brillouin, CEN Saclay, 91191 Gif sur Yvette Cédex, France
|| Laboratory of Solid State Physics, ETH Zürich, CH-8093, Switzerland
¶ LMGP/ENSPG, BP 46, 38402 St Martin d'Hères Cédex, France
†† ISIS Science Division, Rutherford Appleton Laboratory, Chilton, Didcot, Oxon OX11 0QX, UK
‡‡ LSG2M, Ecole des Mines, Parc de Saurupt, 54042 Nancy Cédex, France

Received 8 June 1992, in final form 17 August 1992

Abstract. Perfect single grains of the AlPdMn icosahedral phase have been used for structure determination by x-ray and neutron diffraction. Owing to the large difference between x-ray and neutron scattering factors, information is gained on the atomic positions of the three elements. A model is proposed as deduced from a six-dimensional (6D) Patterson analysis. Six different atomic hypersurfaces are located on node and body-centre sites of the 6D lattice. The superstructure that leads to a face-centred lattice is mainly due to a strong chemical ordering, all the palladium being on the even node and odd body centre of the 6D cube. The resulting 3D structure contains icosahedral clusters similar to the external shell of the Mackay icosahedron, with two kinds of chemical decoration. The structure may also be described via a quasi-periodic stacking of fivefold planes. Each set of planes is characterized by an average chemical composition and local order. This kind of description helps in the understanding of quasi-crystal growth, formation of dislocations and dynamic properties.

1. Introduction

Quasi-crystals are new types of solids that defy previous standard classifications. They are neither periodically ordered, like ordinary crystals, nor disordered or amorphous solids. They have a well defined, discrete group symmetry, like crystals, but one that is explicitly incompatible with three-dimensional (3D) periodic translational order (e.g. exhibiting five-, eight-, or 12-fold symmetry axes). Instead, quasi-crystals possess a novel kind of translational order known as *quasi-periodicity*.

Atomic order is best defined in terms of the Fourier transform of the mass density of the solid. In an ordinary crystal, this transform can be written as a Fourier series:

$$\rho(\boldsymbol{r}) = \frac{1}{V}\sum_{\boldsymbol{G}} \rho(\boldsymbol{G}) \exp(\mathrm{i}\boldsymbol{G}\cdot\boldsymbol{r}). \tag{1}$$

§§ Present address: NIRIM, 1-1 Namiki, Tsukuba, Irabaki 305, Japan.

0953-8984/92/5010149+20$07.50

The set of wavevectors G define a discrete *reciprocal lattice* in which each wavevector in the sum can be written as an integer linear combination of *three* 'basis' vectors a_i^*

$$G = ha_1^* + ka_2^* + la_3^*. \tag{2}$$

The a_i^* are integer linearly independent, which means that $G = 0$ if and only if all the h, k, $l = 0$. The a_i^* are said to span the reciprocal lattice. They are related to the 'basis' vectors a_i that define the unit cell of the crystal in physical space:

$$a_i^* a_j = \begin{cases} 0 & \text{if } i \neq j \\ 2\pi & \text{if } i = j. \end{cases}$$

In a quasi-crystal, the Fourier transform of the mass density is also a Fourier series and the wavevectors in the Fourier sum also form a discrete reciprocal lattice. However, the number of integer linearly independent basis vectors required to 'span' the reciprocal lattice exceeds the spatial dimension, and the point symmetry of the reciprocal lattice is incompatible with periodic translational order. For example, six basis vectors are required to span the reciprocal lattice for three-dimensional quasi-crystals with icosahedral symmetry:

$$G = n_1a_1^* + n_2a_2^* + n_3a_3^* + n_4a_4^* + n_5a_5^* + n_6a_6^* \tag{3}$$

where the a_i^* can be selected to point along the fivefold axes of an icosahedron. In a well chosen cubic coordinate system (i.e. three twofold axes) the a_i^* vectors are of the form $(\pm 1, \pm\tau, 0)$ (and permutations) with $\tau = (1+\sqrt{5})/2 = 2\cos 36° = 1.618\,034\ldots$ the golden mean. Thus, all the vectors G have cubic coordinates of the form $(h+\tau h', k+\tau k', l+\tau l')$ with h, h', k, k', l, l' integral numbers (selected within extinction rules). This is the simplest possible definition of a quasi-crystal. The dense reciprocal space of a quasi-crystal as described by equation (3) may be given a *periodic image* in a high-dimensional space; for instance, equation (3) may be considered as a description of a six-dimensional (6D) periodic reciprocal lattice whose Fourier transform would generate 6D periodic mass density distribution. Projection and cut operation will then relate the physical 3D description to its 6D image.

As a consequence the atomic structure of icosahedral phases is now best understood via a 6D crystallography approach [1–3]. In this scheme, the conventional tools of crystallography, such as Patterson analysis, can be used in the analysis (for a review see [4–7]). It has been shown that the most natural way of analysing such diffraction data is the so-called cut method, as proposed by Bak [8] and Janssen [9], and first applied by Gratias *et al* [10]. Hereby the periodic image space is decomposed into two subspaces, i.e. E_{par}, the physical space, and E_{perp}, the complementary space. The quasi-crystalline structure is defined by a set of atomic hypersurfaces that decorates the 6D cube. The purpose of any structural determination thus reduces to (i) locating the different atomic hypersurfaces and (ii) determining their precise volumes and shapes. However, atomic hypersurfaces are not point-like objects and would require the determination of an infinite number of parameters in order to be completely specified. A first simplification comes in if contrast variation is feasible, which allows the partial atomic correlations to be disentangled from each other [11–13]. But additional constraints must be also injected into models. The first of these, which is trivial, is atomic density, along with chemical composition and unphysically

short distances in physical space, which have to be avoided. This already limits the set of possible solutions to variation around a common hard core, which represents at least 80–90% of the total structure. Further additional constraints may originate from: (i) forcing the frequency of a selected cluster to a maximum as in the i-AlMnSi model proposed by Duneau and Oguey [14]; and (ii) the so-called closeness condition, which prevents the annihilation–creation of atoms under phason-like translation [15, 16] (as in the i-AlCuFe model proposed by Cornier-Quiquandon *et al* [17]).

Following considerations on possible growth mechanisms of quasi-crystals, it has been suggested that real quasi-crystals should be described by random tiling models (as opposed to the perfect quasi-crystal description). Phason fluctuations (corresponding to tile rearrangements or atomic jumps) would result in structures entropically stabilized at high temperature [18–20]. In such models, sharp Bragg reflections are still present, but phason fluctuations cause diffuse rings around peaks, whose intensity scales with Q_{perp}. A systematic measurement of the weak diffuse x-ray scattering around strong Bragg peaks of an annealed AlCuFe single quasi-crystal has been done recently by Mori *et al* [21]. They did not find any Q_{perp}-dependent diffuse scattering, which implies that phason fluctuations, if any, are very small.

The best candidates for structure determination from diffraction data are the recently discovered phason-free, 'perfect', stable quasi-crystals AlCuT (T = Fe, Ru, Os) and AlPdT (T = Mn, Re) [22–24]. The width of the Bragg reflections, when measured on a high-resolution diffractometer, is limited only by instrumental resolution and does not show the broadening expected from quenched-in phason strain [25–27].

This paper reports on a single-crystal x-ray and neutron diffraction study of the i-AlPdMn phase. Contrast variations on Mn sites have previously been measured with powder neutron diffraction techniques, leading to positions and raw shapes of atomic surfaces corresponding to (AlPd) versus Mn atoms [28]. However, powder samples do not allow one to measure properly the degenerate reflections (having the same $|Q|$, but different orbits). Moreover, distinction between Al and Pd sites is difficult in measurements made by neutron diffraction, owing to similar scattering lengths of Al and Pd. The use of both x-rays and neutrons is particularly attractive, since x-rays will mainly probe Pd order, whereas neutrons will probe Mn order. The situation is similar to the AlLiCu quasi-crystals, for which models have recently been proposed [13, 29, 30], and much more favourable than for AlFeCu, for which only weak contrast effects can be expected [17].

2. X-ray data

Large single grains of the AlPdMn icosahedral phase were obtained by the conventional Bridgman growth technique [27]. Spherical grains with approximate radius of 140 μm were cut and set on the tip of a glass fibre for the purpose of single-crystal x-ray diffraction measurements. The sample was fully characterized to be of perfect quasi-crystallinity, i.e. without any detectable quenched-in phason strain, and single phase. The composition was determined by electron probe analysis and found to be equal to $Al_{68.7}Pd_{21.7}Mn_{9.6}$ [27]. The measured density is 5.1 ($\pm$0.2) g cm^{-3}. Figure 1 shows typical x-ray Laue transmission diffraction patterns taken along the twofold, fivefold and threefold directions.

Data collection was performed with a Nicolet four-circle diffractometer equipped with a molybdenum x-ray tube (λ = 0.7107 Å). Integrated intensities were collected

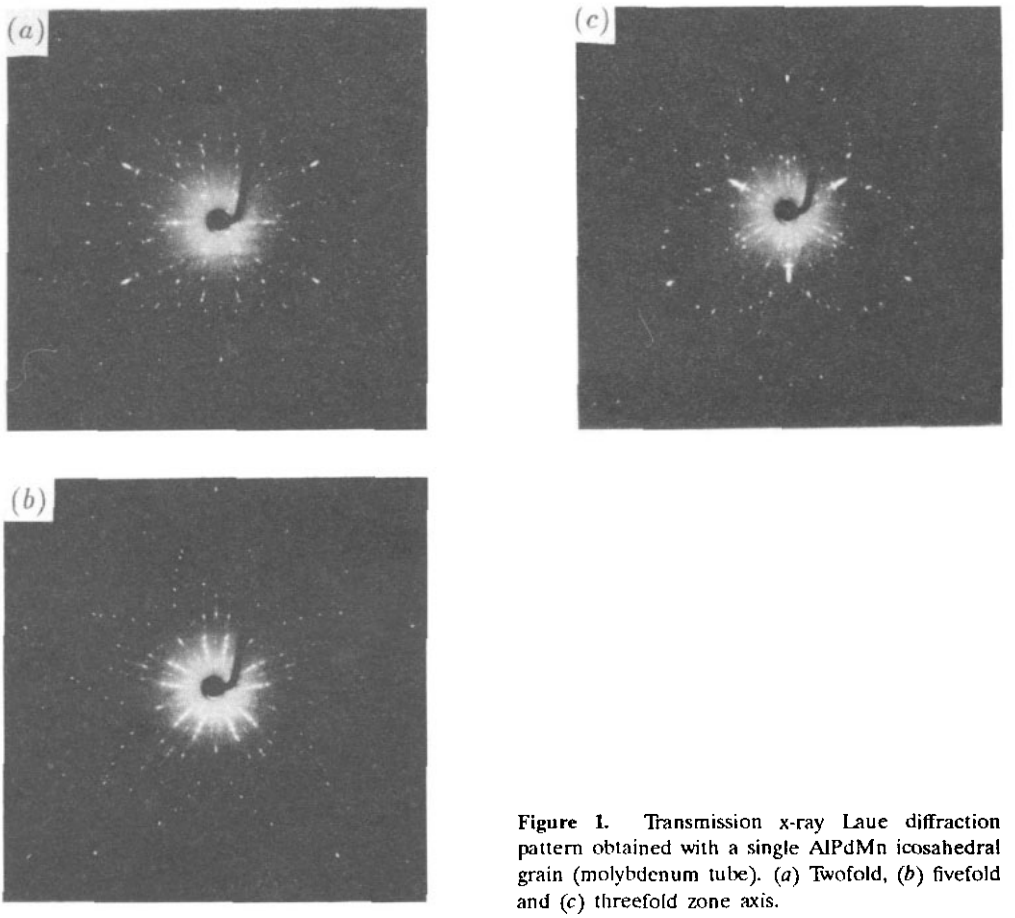

Figure 1. Transmission x-ray Laue diffraction pattern obtained with a single AlPdMn icosahedral grain (molybdenum tube). (*a*) Twofold, (*b*) fivefold and (*c*) threefold zone axis.

by ω scan of the Bragg reflections. A total of 600 reflections were measured in the asymmetric unit, 360 of which with intensities I greater than twice the standard deviation $\sigma(I)$. The region of reciprocal space scanned corresponded to Q_{par} up to 10 Å^{-1} and Q_{perp} up to 1.5 Å^{-1}, with an almost constant resolution equal to 0.08 Å^{-1} [31].

A subset of 120 reflections was selected in order to check their equivalence under the icosahedral point group: fluctuations beyond statistics were not observed, except for a few cases for which absorption, extinction and/or multiple scattering effects may be involved. The ψ scans, in which the sample is rotated around the reciprocal vector, did not show either any fluctuations greater than the statistical ones. Laue (if any) and fluorescence effects were accounted for by subtracting a flat background under each peak. Integrated intensities were then corrected for absorption and Lorentz polarization. A short report on part of these x-ray data has been presented previously and is being published in conference proceedings [31].

3. Neutron data

3.1. Single-crystal data

An ingot with nominal composition $Al_{70}Pd_{21}Mn_9$ was prepared from the pure element

in a plasma jet furnace. It was then sealed in a quartz cell and annealed for 3 days at 800 °C, and then quenched in liquid nitrogen. The annealed ingots were crushed into two or three pieces. It was observed that the specimens showed a crystal-like planar cleavage, and the newly obtained surfaces were flat and had a mirror-like reflectivity. Electron channelling patterns (ECP) showed that the cleaved surfaces are usually normal to a fivefold axis. However, surfaces normal to a twofold axis or to a threefold axis were also observed. The single quasi-crystal selected for neutron diffraction measurements is presented in figure 2(*a*). The surface observed is normal to a fivefold axis as indicated by ECP (figure 2(*b*)). Along the line underlined by two arrows in figure 2(*a*) the quasi-crystal unit was separated from the rest of the ingot by cleavage. The orientation of the newly obtained flat surface was determined by an ECP and was found to be normal to a twofold axis (figure 2(*c*)) [32].

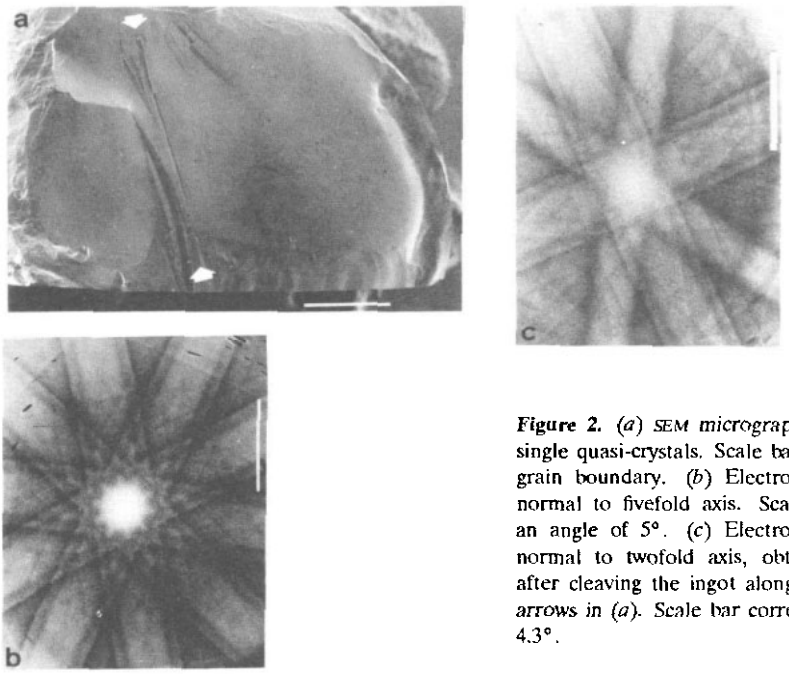

Figure 2. (*a*) SEM micrograph of large Al–Mn–Pd single quasi-crystals. Scale bar 1 mm. Arrows mark grain boundary. (*b*) Electron channelling pattern normal to fivefold axis. Scale bar corresponds to an angle of 5°. (*c*) Electron channelling pattern normal to twofold axis, obtained on the surface after cleaving the ingot along the line indicated by arrows in (*a*). Scale bar corresponds to an angle of 4.3°.

Four-circle neutron diffraction data were collected at the 5C2 instrument located on a hot beam of the Orphée Reactor (Léon Brillouin Laboratory). The beam is monochromatized to $\lambda = 0.8308$ Å with a Cu [2 2 0] monochromator. A systematic search for Bragg reflections did not show any subsidiary grains.

The data collected correspond to ω scans between 5° and 30° and to $\omega - 2\theta$ scans for angles greater than 30° ($Q_{par} < 11.8$ Å^{-1} and $Q_{perp} < 0.95$ Å^{-1}). The resolution is almost constant and equal to 0.08 Å^{-1}. A total of 434 Bragg reflections were measured in the asymmetric unit. A subset of 192 peaks have intensities greater than $2\sigma(I)$. Each reflection was measured three times by application of the threefold rotation; fluctuations greater than the statistical ones were not detected.

3.2. High-resolution powder diffraction data

An ingot with nominal composition $Al_{71}Pd_{19}Mn_{10}$ was prepared by induction melting and solidified in a water-cooled crucible. The ingot was then ground into a fine

powder for the purpose of high-resolution powder neutron diffraction measurements. Data were collected at the Intense Pulsed Neutron Source (ISIS, Rutherford Appleton Laboratory) on the time-of-flight HRPD diffractometer. The apparatus was set in back-scattering configuration resulting in a constant $\Delta Q_{par}/Q_{par}$ resolution equal to 0.0008, i.e. one to two orders of magnitude better than for the above four-circle experiment. The accessible Q_{par} ranged from 1 to 12 Å^{-1}. Advantages of powder diffraction are twofold:

(i) All the reciprocal space is scanned, which allows one to check that no reflection was missed when performing the four-circle experiment. In fact scanning systematically all the reciprocal space is impossible in a four-circle experiment, owing to the reciprocal space of an icosahedral structure being densely filled. Practically only those reflections which have a Q_{perp} value lower than a threshold are effectively measured in a four-circle experiment.

(ii) The high resolution allows one to make accurate measurements of possible quenched-in phason strain.

A typical powder diffraction pattern is shown in figure 3. All the peaks can be indexed according to the scheme proposed by Cahn *et al* [33] and have effectively been measured in four-circle experiments. The peak widths are slightly larger than the instrumental resolution, but do not show any obvious Q_{perp} dependence (figure 4). By contrast, similar samples obtained by the melt spinning technique exhibited a very strong Q_{perp} dependence. Peaks were fitted by pseudo-Voigt functions convoluted with the instrumental resolution, using the ISIS software package [34]. Owing to the very good resolution and the large Q-range accessible, the integrated intensities of 106 reflections were measured, which corresponds to 171 independent reflections.

Finally, it has to be emphasized that, for all experimental data presented here, Q_{perp}-dependent diffuse scattering was not observed and the lineshape of Bragg reflections did not depend on Q_{perp} in any of these neutron and x-ray experiments. This means that, even if this quasi-crystal is of a random tiling type, phason fluctuations are small enough for a description in terms of a perfect quasi-crystal to be completely adequate.

4. From diffraction data to the six-dimensional structure

The first step in diffraction data analysis consists of finding the Bravais lattice and the unit-cell parameter. As already shown for AlCuFe [35, 36] and AlPdMn samples [37], the reciprocal lattice is body-centred. The indices fall into two categories, i.e. all odd or all even 6D indices. However, the intensities of Bragg reflections corresponding to all odd indices are weak, so that the reciprocal space is best described by a primitive cubic lattice with a set of superstructure reflections with their indices all half-integers [36]. This corresponds to a primitive cubic unit cell in direct space with a parameter $a = 6.451$ Å, and two families of lattice nodes, even or odd, where the parity refers to that of the sum of the six corresponding coordinates. The superstructure is induced by small differences in atomic hypersurface shapes, volumes and/or chemical species involved. No other extinction than the one originating from the BCC reciprocal lattice has been observed, so that the space group is either $Fm\bar{3}\bar{5}$ or $F235$ (centrosymmetric or non-centrosymmetric) [38]. In the following, lattice nodes of interest are going to be labelled n_0 and n_1, with 6D coordinates [000000] and [100000] respectively.

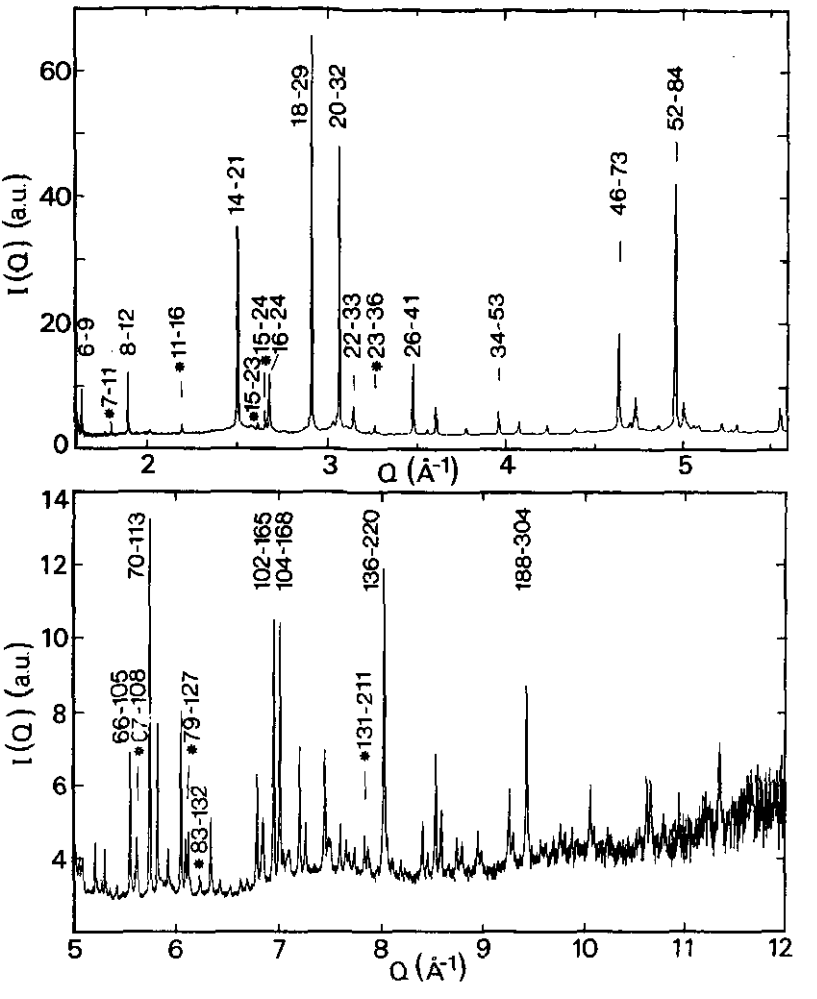

Figure 3. High-resolution powder diffraction pattern. Main Bragg reflections are indexed following the indexing scheme proposed by Cahn *et al* [33].

Body-centre sites with 6D cordinates $\frac{1}{2}[1\,1\,1\,1\,1\,1]$ and $\frac{1}{2}[1\,1\,1\,1\,1\,\bar{1}]$ will also be given labels, i.e. bc_0 and bc_1, respectively.

4.1. The six-dimensional Patterson analysis

As for any periodic distribution of density, the 6D Fourier transform of the peak integrated intensities measured with quasi-crystals gives a 6D Patterson function. It corresponds to the autocorrelation function of the time-averaged density. For a monatomic system, one can write

$$I(Q) = |u(Q)|^2 |F(Q)|^2 \tag{4}$$

where $u(Q)$ is related to the interaction mechanism between one atom and the radiation used. For instance $|u(Q)|^2$ is the atomic scattering factor (or form factor)

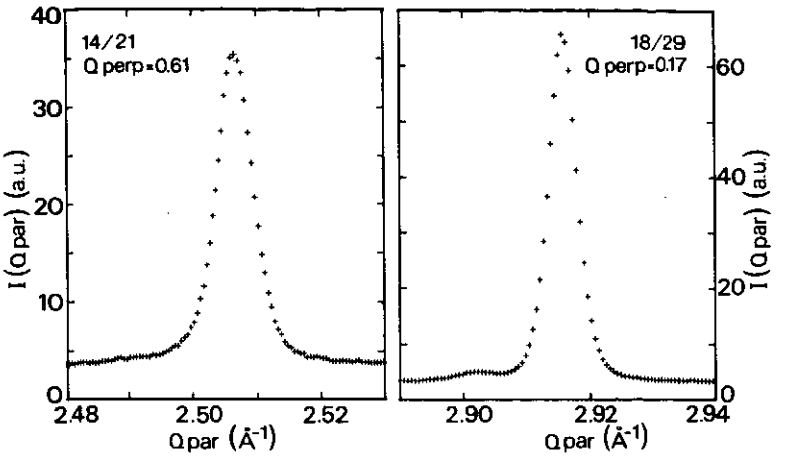

Figure 4. Enlarged part of figure 3, showing two Bragg reflections with their Q_{perp} value in a 3:1 ratio. There is no significant broadening.

f for x-rays and the scattering length b for neutrons. $F(Q)$ is the structure factor, related to the Patterson function $P(r)$ via the expression

$$|F(Q)|^2 = \int P(r) \exp(-iQ \cdot r)\, dr$$

with

$$P(r) = \frac{1}{N} \int \rho(r')\rho(r' + r)\, dr' = \langle \rho(0)^* \rho(r) \rangle. \tag{5}$$

Here N is the number of atoms in the sample, $\rho(r)$ the mass density function, and $*$ means convolution product.

In a polyatomic system, partial Patterson functions can be defined in a similar way:

$$P_{ij}(r) = \frac{1}{N_i} \int \rho_i(r)\rho_j(r' + r)\, dr' = \langle \rho_i(0)^* \rho_j(r) \rangle. \tag{6}$$

Then, the Fourier transform of the peak integrated intensities is a linear combination of the $P_{ij}(r)$, weighted by the product $f_i f_j$ (for x-rays) or $b_i b_j$ (for neutrons). This weighted sum of the partial Patterson functions is usually referred to as the 'total Patterson function' (TPF). The b_i are constant parameters but the x-ray atomic form factors are Q-dependent. This is crudely accounted for by normalizing the x-ray integrated intensities to the mean square value of the atomic form factor defined as:

$$\langle f^2 \rangle = \sum_i c_i f_i^2$$

where c_i are concentrations of the atomic species in the material. Conclusively, the Fourier transforms of the intensities of the x-ray (neutron) diffraction peaks properly indexed in the 6D scheme give a set of TPF such as:

$$\text{TPF} = \sum_{ij} f_i f_j (b_i b_j) P_{ij}(r) \tag{7}$$

($f_i f_j$ for x-rays, $b_i b_j$ for neutrons).

Figure 5 reproduces a planar slice of 6D TPF examples, containing two fivefold axes taken in the physical 3D space for one and in the complementary space for the other. The TPF features appear as traces, elongated on the perpendicular space axis. Their actual width in the physical space is mainly due to truncation effects in the Fourier transform procedure. These observations hold true for any 2D slice of the 6D TPF, which means that the TPF features are basically 3D full 'objects' in the perpendicular space, with point-like intersection with the physical space. These TPF 'objects' have centres that are located at four positions only, namely n_0, n_1, bc_0 and bc_1 (see figure 5). This corresponds to atomic hypersurfaces whose centres can also only be in positions n_0, n_1, bc_0 and bc_1, i.e. at points with very high symmetry in the 6D cubic lattice. This solution is centrosymmetric, although in principle Patterson functions do not give information on whether the structure is centrosymmetric or not. It just happens here that the only structural solution compatible with the measured TPF is a centrosymmetric one, in agreement with contrast variation effects [28]. To be fair, the point is not universally accepted. Recently, Lee *et al* [39] have measured directly the phase differences of the structure factors, using dynamic Renninger effects, on an AlCuFe sample whose atomic structure is similar to that of AlPdMn. Their result deviates significantly from a centrosymmetric solution. (It has to be noted, however, that the theoretical treatment used by these authors may not be applicable to quasi-crystalline cases.) A possibility might be that the shape of the atomic hypersurfaces is not centrosymmetric: this cannot be ruled out by the Patterson analysis, but the non-centrosymmetric character, if any, can be only very weak.

Looking back now at equation (7), it can be expected that TPF reflect mainly the density distribution related to atoms with strong $f_i(b_i)$. In the present case, TPF obtained from x-ray data are certainly reflecting palladium distribution in the structure, since $Z_{Pd} = 46$ compared to $Z_{Mn} = 25$ and $Z_{Al} = 13$. The TPF obtained from neutron data are not very sensitive to Pd versus (Al, Mn) order but heteroatomic correlation with Mn has a negative contribution to the TPF owing to its negative scattering length ($b_{Mn} = -0.373$ while $b_{Al} = 0.3449$ and $b_{Pd} = 0.591$ 10^{-12} cm). This is actually exemplified with profiles of the density–density correlations, resulting from planar cuts of the TPF in the perpendicular space and illustrated in figure 6. These profiles show clearly that the TPF maxima centred at n_0, n_1, bc_0 and bc_1 result from *large* atomic hypersurfaces centred at n_0 and n_1, plus *small* atomic hypersurfaces centred at bc_0 and bc_1 [28]. Some chemical order effects appear in slope changes (figure 6(*b*)) for profiles of the TPF maxima, which are deduced from neutron data: the inner core of atomic hypersurfaces located at n_0 and n_1 corresponds to manganese atoms while an outer shell contains the contribution from Al and/or Pd. Moreover, a large difference in density–density correlations between n_0 and n_1 TPF maxima shows up when obtained from x-ray data (figure 6(*a*)); it is consistent with the Pd atoms contributing to the outer shell of the n_0 atomic hypersurface but not to the n_1 one. The large density–density correlations showing up at the bc_1 position in the TPF deduced from x-ray data indicates that Pd atoms contribute also to the atomic hypersurface located at bc_1 [31]. These results, together with the powder neutron contrast variation experiment [28], where the size of the Mn atomic surfaces has been determined, lead to a crude model that is described in the following section.

4.2. A crude modelling

Reasonably founded information about the size of the different atomic hypersurfaces

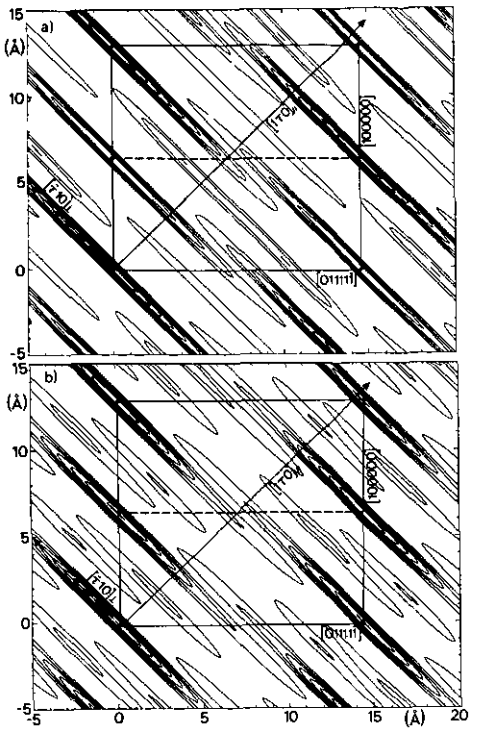

Figure 5. Rational cut of the 6D Patterson function, in a plane containing a fivefold axis in both the physical and the perpendicular space, as deduced from single-crystal x-ray (*a*) and neutron (*b*) diffraction data. The primitive unit cell is outlined.

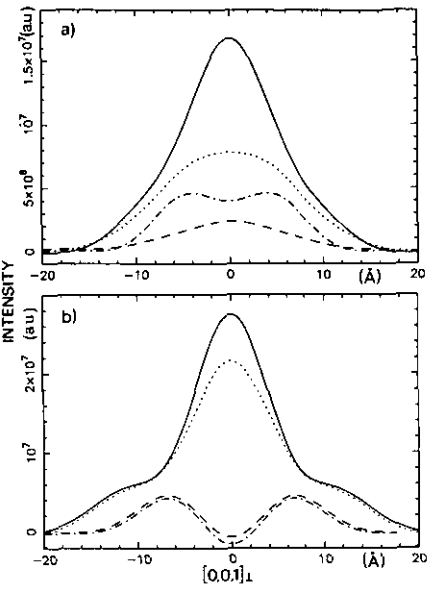

Figure 6. Profiles of the various Patterson density features on even (——) or odd (·····) lattice nodes, and on even (- - - -) or odd (— · —) body centres as deduced from x-ray (*a*) and neutron (*b*) data. The large difference between odd and even lattice-node profiles obtained from x-ray data is due to chemical ordering, Pd being located on n_0.

may result from models using balls and spherical shells. Actually, at small values of Q_{perp} (i.e. smaller than 0.5 Å^{-1}), the Fourier transform of an atomic hypersurface is mainly influenced by its size and does not depend on its precise shape. This is illustrated in figure 7, where the Q_{perp} dependence of the amplitude of the structure factor $|F(Q)|$ (square root of the intensity, corrected for absorption, Lorentz polarization and Debye–Waller factor) is shown. Had we had to consider one single atomic hypersurface in the 6D structure (simple cubic primitive lattice) $F(Q)$ would have been proportional to $G(Q_{perp})$, the Fourier transform of the atomic hypersurface. It is a smooth decaying function at low values of Q_{perp}. In the present case, several (say n) atomic hypersurfaces have to be considered and we must express $F(Q)$ as

$$F(Q) = \sum_{l=1}^{n} b_l G_l(Q_{perp}) \exp(-iQ \cdot R_l). \tag{8}$$

R_l are the space positions of the centres of the atomic hypersurfaces in the 6D cubic unit cell; b_l is for neutron scattering length and must be replaced by f_l when x-rays are concerned. The R_l-vectors are only 6D lattice vectors (n_0, n_1) or 'half'

6D lattice vectors (bc_0, bc_1). The Q-vectors correspond to the Bragg peaks indexed in the 6D reciprocal space. They belong to two principal families, corresponding either to primitive (strong) reflections with all integer indices (even reflection such as (000000) or odd reflection such as (000001)) or to superstructure (weak) reflections with all half-integer indices (integers are again either even or odd). The parity on the reflection indices is transferred to the Q_{par} and Q_{perp} modulus via the parameters N and M, as defined elsewhere [17,33]. The consequence of $\boldsymbol{R}_l$ and $\boldsymbol{Q}$ having special forms is that $\exp(-i\boldsymbol{Q}\cdot\boldsymbol{R}_l)$ in equation (8) takes only values ± 1. Thus, rewriting $C_l = b_l G_l(\boldsymbol{Q}_{perp})$ for brevity, equation (8) has the general form

$$F(\boldsymbol{Q}) = \sum_l \pm C_l. \tag{9}$$

(Each C_l contains possibly several contributions if the global atomic hypersurfaces at position R_l have to be decomposed into component volumes corresponding to different atomic species.) There are only four alternatives for equation (9), i.e. [17]:

(i) even primitive reflections $F(\boldsymbol{Q}) = +C_{n_0} + C_{n_1} + C_{bc_0} + C_{bc_1}$;
(ii) odd primitive reflections $F(\boldsymbol{Q}) = +C_{n_0} + C_{n_1} - C_{bc_0} - C_{bc_1}$;
(iii) even superstructure reflections $F(\boldsymbol{Q}) = +C_{n_0} - C_{n_1} + C_{bc_0} - C_{bc_1}$;
(iv) odd superstructure reflections $F(\boldsymbol{Q}) = +C_{n_0} - C_{n_1} - C_{bc_0} + C_{bc_1}$.

Thus, the Q_{perp} dependence of the structure factor splits into four families as shown in figure 7. Four such branches have been observed previously with AlCuFe single-crystal data [17] and AlPdMn powder data [28]. The next step in the interpretation of the data is to fit the low-Q_{perp} parts of these four branches with $G_l(Q_{perp})$ functions (equations (8) and (9)) corresponding to balls and/or spherical shells. As a first approximation, atomic hypersurfaces have been supposed to lie in the perpendicular space. This hypothesis is compatible with the observed TPF whose traces in slices (figure 5) of the 6D space appear to be confined in 'cigar-like' shapes along an axis in perpendicular direct space. One should note, however, that a small parallel component (i.e. lower than 0.6 Å) would hardly be recognized on a density or Patterson map because of smearing truncation effects [40]. Within density and chemical composition constraints, the best fit to low-Q_{perp} data of the four $F(Q)$ branches was obtained with atomic hypersurfaces defined as follows:

(i) A core of Mn (radius $0.83a$, where a is the parameter of the 6D cube) surrounded by an intermediate shell of Pd (extending up to $1.26a$) and an outer shell of Al (up to $1.55a$) centred at n_0 position.

(ii) A core of Mn (radius $0.52a$, about 1.6 times smaller than the one on the n_0 node) surrounded by a shell of Al (up to $1.64a$, i.e. larger than the n_0 one) but without palladium, centred at the n_1 position.

(iii) A ball of Pd (radius $0.71a$) at bc_1 position.

(iv) A small ball of Al (radius $0.3a$) or an empty volume at bc_0 position. (The fit did not show differences between these two hypotheses since the Al volume involved is very small.)

Such a crude spherical model is found to fit the data relatively well and results in residual R-factors of 9% for x-ray and 16% for neutron data when considering reflections with $Q_{perp} < 0.5$ Å^{-1}. Such R-factors would be considered as relatively poor in classical crystallography. But there are actually no published models that,

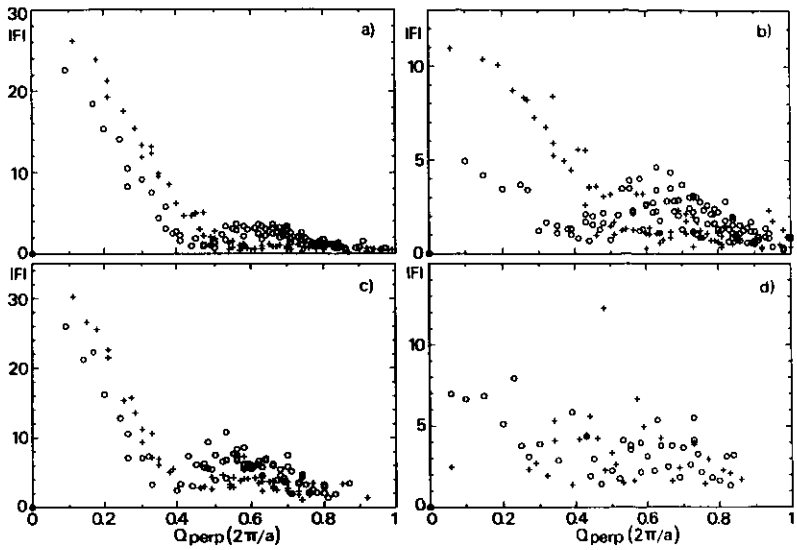

Figure 7. Q_{perp} dependence of the structure factors for x-ray (a, b) and neutron (c, d) data. X-ray data were normalized to the mean value of the atomic scattering factor (which is Q_{par}-dependent), and both data were corrected by a mean Debye–Waller factor. In both cases each set of primitive reflections (a), (c), corresponding to $N = 2p$ decomposes in two branches according to the parity of M ($+M$ even, 0 M odd). For superstructure reflections (b), (d), corresponding to $N = 2p+1$ a similar decomposition is seen (0 M even, $+M$ odd). N and M refer to the indexing scheme proposed by Cahn *et al* [33] and are directly related to the reflection parity [17].

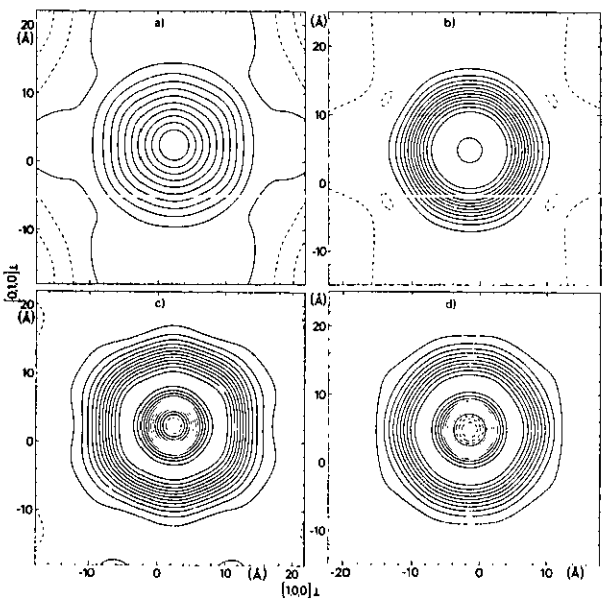

Figure 8. Contour plot of different sites observed in the Patterson function. The representation is in the perpendicular space. Even and odd body-centre sites obtained with x-ray (a), (b) and neutron (c), (d) data. The coordinate axes and the perpendicular to the figures are twofold axes in the complementary (perp) space.

to our knowledge, would better fit x-ray and neutron data altogether. The fit of the present crude model to high-order weaker reflections appears to be not that bad

(*R*-factor of 11% and 20% for x-rays and neutrons respectively). Clearly, to improve the fit to both low- and high-order reflections, facetting of the atomic hypersurfaces has to be introduced. This search may somehow be guided by the shape of the TPF maxima when looked at in perpendicular space. In some cases this function exhibits visible facetting (figure 8). In principle the shape of the density–density correlations is complicated since it originates from the self-overlapping of different atomic hypersurfaces with different weight corresponding to the scattering length of the atom. However, in the present case, as noticed by Cornier-Quiquandon *et al* [17], the relatively small atomic hypersurface located at the body-centre position acts as a probe. When looking at the body-centre density–density correlation, in the TPF map, information is mainly obtained about the shape of atomic hypersurfaces sited at n_0 or n_1. This probe is more efficient when the scattering lengths of elements are close to each other, as is the case for neutron diffraction data where b_{Al} and b_{Pd} are closer to each other than with x-rays. Effectively, a facetting is seen in figures 8(*c*) and (*d*), where in one case there is a bump along the fivefold axis and a depression along the threefold axis as for an icosahedron, whereas in the other case contours are reminiscent of a triacontahedron. This is probably an indication of differences in the external shape of the two n_0 and n_1 atomic hypersurfaces similar to those in the AlCuFe quasi-crystal [17].

Pushing the interpretation of the facettings exhibited in figure 8 to its extreme, it is probably tempting to suggest that:

(i) The atomic surface corresponding to the Mn core at n_0 position has a triacontahedral shape.

(ii) The Mn core is a dodecahedron at n_1 position.

But this is only very tentative and must be confirmed further in the future.

An alternative approach is to fit the data with atomic hypersurfaces that are composed by superimposing spherical harmonics of icosahedral symmetry [41]. It has been applied successfully to our diffraction data measured with AlCuLi quasi-crystals [13]. This looks very promising and is in progress for the present system.

For comparison, the present data were also confronted with three other types of models, in their simplified 'spherical' version:

(i) A modified Duneau–Oguey description [14]. The main difference concerns small atomic surfaces that are located at the mid-edge of the 6D cube.

(ii) A structure similar to that found experimentally for the AlMnSi quasi-crystal [12]. In both models the atomic surfaces have identical external shell on n_0 and n_1 lattice nodes and a relatively small body-centre atomic surface. The FCC superstructure has exclusively a chemical origin.

(iii) A model similar to that proposed for AlCuFe quasi-crystal, where superstructure originates from both chemical and crystallographic order [17].

Globally, these three descriptions are less adequate than the previous one. Models (i) and (ii) exhibit a too-small body-centre site when compared to Patterson functions, whereas model (iii) induces too weak a mass density (0.060 atom/Å^3 instead of 0.066 atom/Å^3).

The density problem in (iii) has recently been corrected [42] in a modified model. It may fit closer to the present data.

Isotopic substitution on Cu and Fe in AlFeCu quasi-crystals [42] has also shown some evidence of chemical order that compares reasonably well with the one proposed

in the present work for AlPdMn. Iron contributes to cores of atomic hypersurfaces sited at n_0 and n_1 positions. Shells of copper appear at n_0, but also at n_1, and there is a 'ball' of copper at bc_1. Outer shells of Al are visible at n_0 and n_1. The position bc_0 is unoccupied. The Al shells are partially mixed with iron. Conclusively, differences with the present analysis come from (i) Al–Fe partial disorder while Al–Mn are not mixed, (ii) Cu cores are sited at both n_0 and n_1 while Pd is only at n_0, and (iii) Fe cores have equal sizes at n_0 and n_1 while Mn cores have not.

Finally, it is interesting to wonder how far such a spherical model is from the 'true' solution. As has been pointed out repeatedly, since atomic hypersurfaces need an infinite number of parameters to be completely specified, there will be an infinite number of models fitting equally well the same (finite) set of data. However, models must have a common 'hard core', which represents at least 80–90% of the total number of atoms [7, 43]. This is mainly due to the constraint imposed by composition and density. The 6D space is widely open but positioning atomic hypersurfaces that reproduce the experimental atomic density and avoid short distances forces solutions in which atomic hypersurfaces are in contact. This strongly restricts the degrees of freedom for modelling. Finally, fitting low-Q_{perp} data may be viewed as a 'low-resolution' image of the icosahedral structure, whereby the term 'low-resolution' refers to perpendicular space. This is reminiscent of current methods of modelling applied in biology for structure determinations of large proteins.

The AlPdMn icosahedral phase belongs to one of the two icosahedral families that are characterized by large atomic hypersurfaces at the lattice node in 6D cubic image and by small ones at the body centre. The main result of the present study has been to specify where the different atomic species are in these two families of atomic hypersurfaces and to give a 'low-resolution' image of the structure.

5. About the resulting three-dimensional structure

As a result of the previous discussion, it is interesting to look at what are the 'basic' or 'hard core' features when generating the 3D structure as a cut through the 6D image. Following what has been done with the AlLiCu quasi-crystal [13], we may seek local icosahedral clusters, or alternatively we can describe the structure in terms of dense atomic planes. This is of particular interest for considerations on crystal growth, dislocations and also physical properties of the quasi-crystalline phase, such as vibrational states and the electronic structure.

The nature of icosahedral clusters that exist in the 3D structure can be found following the procedure proposed by Duneau and Oguey [14]. Comparing the sphere sizes of interest with Duneau–Oguey atomic hypersurfaces, it can be shown that the external shell of a Mackay icosahedron is actually present in the structure. In the i-AlMnSi phase, the Mackay icosahedron decomposes into three shells, namely a small Al icosahedron, a twice larger Mn icosahedron and an Al icosidodecahedron (30 atoms along twofold directions) [44, 45]. In the AlPdMn icosahedral phase the internal small icosahedron is replaced by pieces of an Al dodecahedron. Two kinds of external shells are found, depending on the parity of the high-dimensional lattice node where the cluster centre is sited. In the 6D description the Mn inner core has a radius smaller than the standard triacontahedron; this implies that the resulting 3D large icosahedron is occupied by Mn atoms plus a small number of Al or Pd atoms. The external icosidodecahedron is made of either Al atoms alone or of Al plus Pd

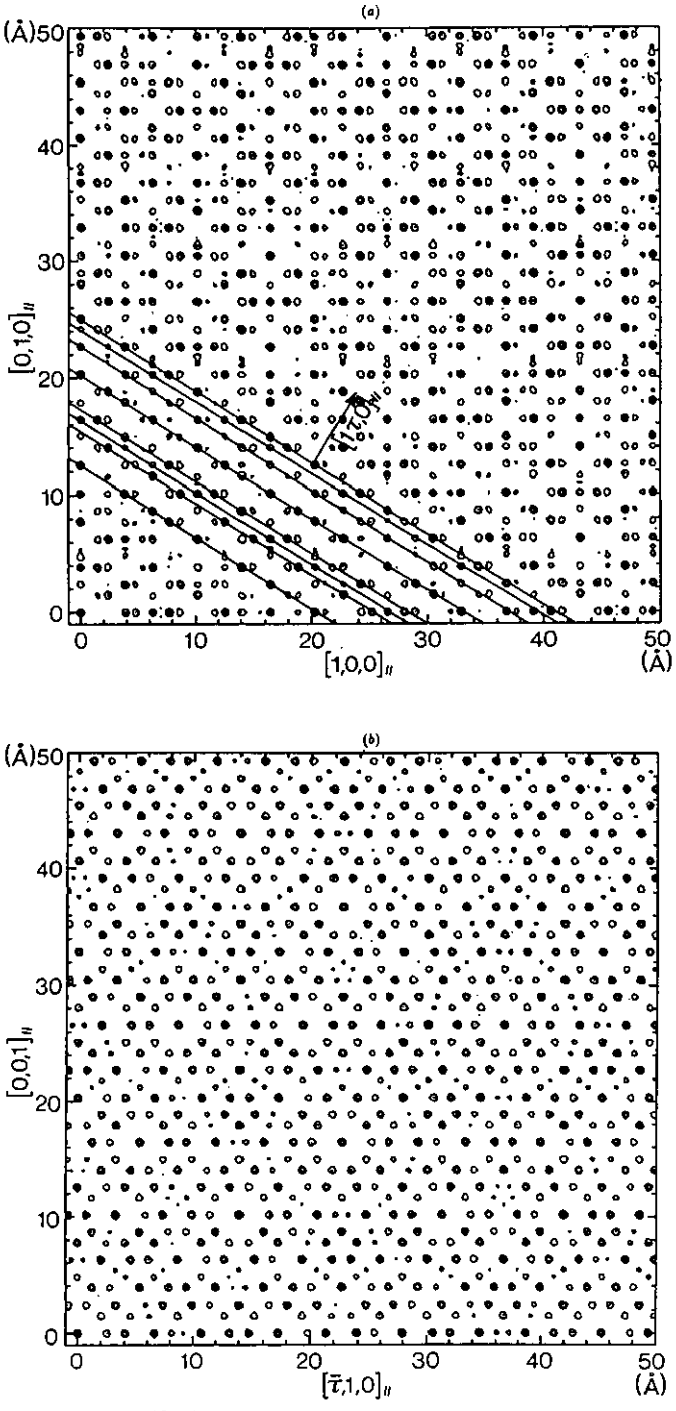

Figure 9. (*a*) Twofold projection of the icosahedral AlPdMn structure as obtained by Fourier transform of the $Q_{par}(Z) = 0$ layer of the reciprocal space. The map shows contour plots of the electronic density. Dense contour regions correspond to high electronic density projection. Densest plans show up perpendicular to the fivefold direction. (*b*) Fivefold projection. This may be compared to high-resolution electron microscopy.

Table 1. Position and chemical composition of a series of atomic planes perpendicular to a fivefold axis. The coordinate Z_{A5} (Å) of each plane, along this fivefold axis, is given, along with the corresponding number of Al, Mn and Pd atoms (N_{Al}, N_{Mn} and N_{Pd} respectively). N_{Tot} is the total number of atoms in the plane. All samples of planes have the same size equal to 100 x 100 Å^2.

Z_{A5} (Å)	N_{Al}	N_{Mn}	N_{Pd}	N_{Tot}	Z_{A5} (Å)	N_{Al}	N_{Mn}	N_{Pd}	N_{Tot}
−21.363	284	207	297	788	2.040	514	0	0	514
−20.881	533	0	0	533	2.522	274	211	303	788
−19.323	792	0	0	792	3.003	49	0	0	49
−18.841	270	48	305	623	3.301	0	0	60	60
−18.062	0	0	174	174	4.080	149	0	0	149
−17.283	269	0	257	526	4.562	827	85	0	912
−16.801	809	33	0	842	5.043	267	0	0	267
−15.243	393	0	0	393	5.822	0	0	105	105
−14.761	268	225	299	792	6.601	274	191	292	757
−14.280	211	0	0	211	7.083	591	0	0	591
−12.721	813	81	0	894	8.641	761	0	0	761
−12.240	272	0	108	380	9.123	261	85	294	640
−11.461	0	0	139	139	9.902	0	0	170	170
−10.682	286	138	305	729	10.681	279	0	196	475
−10.200	662	0	0	662	11.163	807	55	0	862
−8.642	683	0	0	683	12.721	319	0	0	319
−8.160	272	159	298	729	13.203	272	242	301	815
−7.381	0	0	130	130	13.685	290	0	0	290
−6.602	276	0	84	360	15.243	825	60	0	885
−6.120	809	84	0	893	15.725	264	0	183	447
−5.638	16	0	0	16	16.504	0	0	148	148
−4.859	0	0	8	8	17.283	276	107	310	693
−4.562	168	0	0	168	17.765	757	0	0	757
−4.080	275	232	300	807	19.323	602	0	0	602
−3.598	420	0	0	420	19.805	297	184	290	771
−2.040	820	22	0	842	20.584	0	0	115	115
−1.558	273	0	277	550	21.363	282	0	5	287
−0.779	0	0	184	184	21.845	825	83	0	908
0.000	273	25	304	602	22.326	127	0	0	127
0.482	797	0	0	797					

atoms. In summarizing, two types of clusters are present in the physical structure, namely a pseudo-Mackay cluster type 1, with a large icosahedron of Mn + Al and an icosidodecahedron of Pd + Al, and a pseudo-Mackay cluster type 2, with a large icosahedron of Mn + Pd and an icosidodecahedron of Al. Evidences of a hierarchy structure are also observed (big pseudo-Mackay of 'atomic' pseudo-Mackay, etc.).

The existence of densest planes in the 3D structure may be evidenced from planar projections of the structure. This may be obtained either analytically, using the 6D image [46, 47], or by computing the Fourier transform of all structure factors lying in a reciprocal plane, since the Fourier transform of a cut is a projection. Structure factors deduced from x-ray data, together with phases of the spherical model, were used for computation of the twofold projection shown in figure 9(*a*). When looking at this projection at glancing angle, series of lines corresponding to atomic planes are clearly visible. Densest planes are characterized by larger spacing. They are found perpendicular to a fivefold axis. Twofold planes are also visible but they are closer to each other and contain a smaller density of points. Since x-ray structure factors were used, the plots in figure 9 may be compared, in a first approximation, to high-

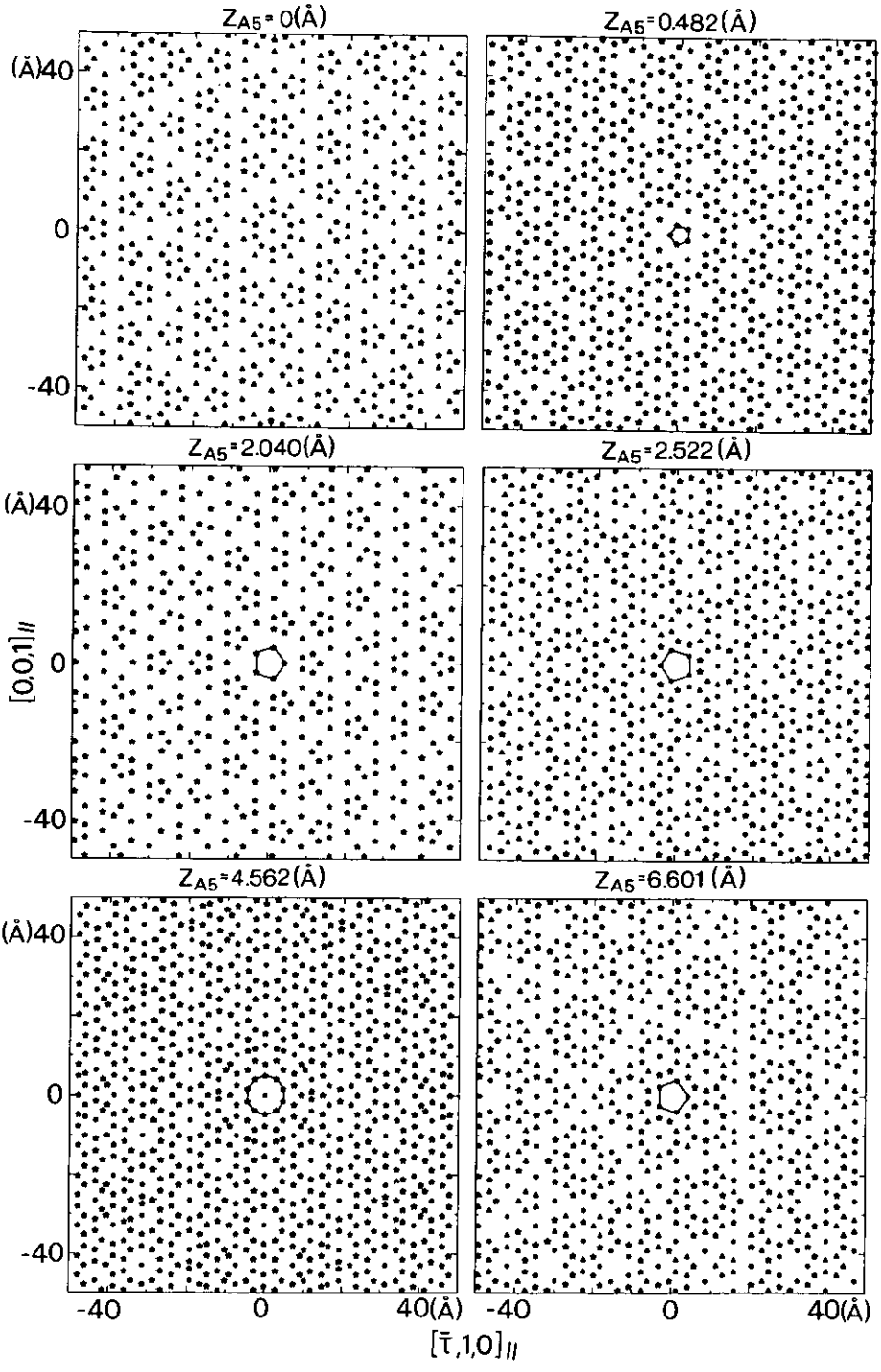

Figure 10. A series of six successive dense atomic planes perpendicular to a fivefold axis. The level of each plane is indicated and can be compared with table 1. Atomic species are indicated: ⁎, Al atoms; ▲, Pd atoms; ●, Mn atoms. Some fivefold rings corresponding to external shells of pseudo-Mackay icosahedra have been outlined.

resolution electron microscopy images. A projection along a fivefold axis is shown in figure 9(*b*).

Two-dimensional cuts of the 3D structure, perpendicular to a fivefold axis and made at different levels along this axis, are pictured in figure 10. A systematic search of the very dense fivefold planes has been carried out. As a result of quasi-periodicity, all planes are in principle different. However, within very small changes in composition and local order, there is only a finite number of different dense atomic planes to be considered. Each 'type' of plane has a similar local order and a chemical composition lying between two close values. All characteristics of dense planes lying in a box of $100 \times 100 \times 50$ Å^3 are gathered in table 1. The coordinates Z_{A5} along the fivefold axis for each plane and the number of Al, Mn and Pd atoms are indicated. For instance, planes located at $Z_{A5} = -20.881$, -15.243, -3.598, 2.040, 7.083, 19.323 Å are all belonging to the same family and containing only Al atoms. Similarly planes located at -21.363, -14.761, -4.080, 2.522, 13.203, 19.805 Å belong to another family and contain Al, Mn and Pd atoms. The largest 'gap' between two successive planes is found to be equal to 1.56 Å (for instance planes at 0.482 Å and 2.04 Å). Some planes are corrugated and consist of one dense plane sandwiched between layers located 0.5 Å apart (for instance plane at 4.562 Å, with two lower-density planes located at 4.08 and 5.043 Å, table 1). Details of the local order will depend on the precise shape of the different atomic surfaces, but the stacking of dense planes is a robust property, which mainly depends on size and average shape of the atomic hypersurfaces.

This description implies a number of straightforward consequences, which may be analysed as follows. In the bulk of the cleaved single quasi-crystals, microholes were observed. These microholes are facetted, with their largest facets perpendicular to a fivefold axis. The most probable equilibrium shape deduced from these observations is the regular Archimedean $\{4, 6, 10\}$ polyhedron [32]. The fivefold facets of this polyhedron are the largest. Similarly to what was found in AlLiCu icosahedral phase [13], equilibrium facets of quasi-crystal may be explained along rules reminiscent of those applied for crystals, i.e. facets are assumed to develop along planes of the highest density. The large distance between fivefold planes is also consistent with the observed easy cleavage, which occurs mainly along the fivefold axes [32]. It is likely that the very different atomic decoration of different planes is important for the stabilization and propagation of the icosahedral order. This description also allows the following prediction to be made, concerning dislocations induced when a strain is applied: if dislocations are mobile, the slip plane should be fivefold plane (densest plane), and the Burgers vector should be perpendicular to a twofold direction, which is the direction of highest density in the fivefold plan following rules usually employed in the analysis of crystal defects. The 6D value of the Burger vector may even be calculated and should correspond to the small lattice spacing that is evident from figure 10.

6. Conclusions

The present single-crystal study has been carried out with single grains of the perfect AlPdMn icosahedral phase, using both x-ray and neutron diffraction. Owing to the large differences between neutron and x-ray scattering lengths of the three elements, information on the chemical order has been obtained. Using the 6D crystallographic

approach, it has been found that there are six different atomic hypersurfaces, which are described by a first-order spherical model, in reasonable agreement with diffraction data. The superstructure on the primitive lattice is concluded to be due to a strong chemical ordering, since all palladium atoms contribute to atomic hypersurfaces located at one of the lattice nodes and one of the body-centre sites. The average structural order of the AlPdMn quasi-crystal, in common with those of the i-AlMnSi and i-AlCuFe phase, exhibits a similar diffraction pattern, and corresponds to a large atomic hypersurface centred at nodes of the 6D cube. Although the proposed crude model is only a first-order approximation, it corresponds to a minimum 'hard core', which will be common to all other possible models. The resulting 3D structure may be described by a quasi-periodic arrangement of icosahedral atomic clusters: the external shell of the Mackay icosahedron is observed, with two kinds of chemical decoration generating the superstructure. It is interesting to consider the structure in terms of dense atomic planes, i.e. a series of different atomic planes, in which each set of planes has about the same local environment and chemical composition. These planes are quasi-periodically stacked perpendicular to a fivefold axis. The existence of these planes is argued here to play an important role in quasi-crystal growth, and also in the possible formation and motion of dislocations. The next step in the structure determination will obviously be to find a more precise shape for the six different atomic surfaces. A guideline for this search is that in the chosen model unphysically short distances must be absent, which will lead to facetted atomic surfaces. The use of the set of atomic surfaces recently proposed by Katz [16], and which obey the closeness condition, may also facilitate this search. In this perspective, precise measurements of density and chemical composition are important and should give rise to specific constraints on sizes of the atomic hypersurfaces, such as those proposed by Kalugin [15, 48].

References

[1] Duneau M and Katz A 1985 *Phys. Rev. Lett.* **54** 2688
[2] Kalugin P A, Kitaev A Y and Levitov L S 1985 *JETP Lett.* **41** 145
[3] Elser V and Henley C L 1985 *Phys. Rev. Lett.* **55** 2883
[4] Janssen T 1988 *Phys. Rep.* **168** 55
[5] Steurer W 1990 *Z. Krist.* **190** 179
[6] Janot C and de Boissieu M 1991 *Quasicrystals: The State of the Art* ed D P DiVincenzo and P J Steinhardt (Singapore: World Scientific) p 57
[7] Guyot P, Kramer P and de Boissieu M 1991 *Rep. Prog. Phys.* **54** 1373
[8] Bak P 1986 *Scr. Metall.* **20** 1199
[9] Janssen T 1986 *Acta Crystallogr.* A **42** 261
[10] Gratias D, Cahn J W and Mozer B 1988 *Phys. Rev.* B **38** 1643
[11] Janot C, Pannetier J, Dubois J M and de Boissieu M 1989 *Phys. Rev. Lett.* **62** 450
[12] Janot C, de Boissieu M, Dubois J M and Pannetier J 1989 *J. Phys.: Condens. Matter* **1** 1029
[13] de Boissieu M, Janot C, Dubois J M, Audier M and Dubost B 1991 *J. Phys.: Condens. Matter* **3** 1
[14] Duneau M and Oguey C 1989 *J. Physique* **50** 135
[15] Kalugin P A 1989 *Europhys. Lett.* **9** 545
[16] Katz A 1990 *Number Theory and Physics* ed J M Luck, P Moussa, M Waldschmidt and C Itzykson (Berlin: Springer) p 100
[17] Cornier-Quiquandon M, Quivy M, Lefebvre S, Elkaim E, Heger G, Katz A and Gratias D 1991 *Phys. Rev.* B **44** 2071
[18] Elser V 1989 *Aperiodic Crystals* ed M V Jaric (New York: Academic) p 105
[19] Henley C L 1991 *Phys. Rev.* B **43** 993

[20] Henley C L 1991 *Quasicrystals: The State of the Art* ed D P DiVincenzo and P J Steinhardt (Singapore: World Scientific) p 429
[21] Mori M, Ishimasa T and Kashiwase Y 1991 *Phil. Mag. Lett.* **64** 49
[22] Tsai A-P, Inoue A and Masumoto T 1988 *Mater. Trans. Japan. Inst. Metals* **29** 521
[23] Tsai A-P, Inoue A, Yokoyama Y and Masumoto T 1990 *Phil. Mag. Lett.* **61(1)** 9
[24] Tsai A-P, Inoue A, Yokoyama Y and Masumoto T 1990 *Mater. Trans. Japan. Inst. Metals* **31** 98
[25] Guryan C A, Goldman A I, Stephens P W, Hiraga K, Tsai A-P, Inoue A and Masumoto T 1989 *Phys. Rev. Lett.* **62** 2409
[26] Bessière M, Quivy A, Lefebvre S, Devaud-Rzepski J and Calvayrac Y 1991 *J. Physique I* **1** 1823
[27] de Boissieu M, Durand-Charre M, Bastie P, Carabelli A, Boudard M, Bessière M, Lefebvre S, Janot C and Audier M 1992 *Phil. Mag. Lett.* **65** 147
[28] Boudard M, de Boissieu M, Janot C, Dubois J M and Dong C 1991 *Phil. Mag. Lett.* **64** 197
[29] Van Smaalen S, De Boer J L and Shen Y 1991 *Phys. Rev.* B **43** 929
[30] Yamamoto A 1992 *Phys. Rev.* B **45** 5217
[31] Janot C, Boudard M, de Boissieu M, Durand M, Vincent H, Dubois J M and Dong C 1991 *J. Non-Cryst. Solids* at press
[32] Beeli C 1992 *PhD Thesis* ETH, Zürich
[33] Cahn J W, Shechtman D and Gratias D 1986 *J. Mater. Res.* **1** 13
[34] David W I F 1988 *Rutherford Appleton Laboratory Report* RAL-88-103
[35] Ebalard S and Spaepen F 1989 *J. Mater. Res.* **4** 39
[36] Devaud-Rzepski J, Quivy A, Calvayrac Y, Cornier-Quiquandon M and Gratias D 1989 *Phil. Mag.* B **60** 855
[37] Tsai A-P, Inoue A and Masumoto T 1990 *Phil. Mag. Lett.* **62(2)** 95
[38] Levitov L S and Rhyner J 1988 *J. Physique* **49** 1835
[39] Lee H, Collela R and Chapman L D 1992 *Preprint* Purdue University
[40] de Boissieu M, Janot C and Dubois J M 1990 *J. Phys.: Condens. Matter* **2** 2499
[41] Elcoro L, Perez-Mato J M and Madariaga G 1992 *Proc. 4th Int. Conf. on Quasicrystals (St Louis, 1992); J. Non Cryst. Solids* at press
[42] Mozer B, Bellissent R, Calvayrac Y, Cornier Quiquandon M, Cahn J W and Gratias D 1992 *Proc. 4th Int. Conf. on Quasicrystals (St Louis, 1992); J. Non-Cryst. Solids* at press
[43] de Boissieu M 1989 *Thèse* INPL, Nancy
[44] Mackay A L 1962 *Acta Crystallogr.* **15** 916
[45] Cooper M and Robinson K 1966 *Acta Crystallogr.* **20** 614
[46] Katz A and Duneau M 1986 *J. Physique* **47** 191
[47] Shaw L J, Elser V and Henley C L 1991 *Phys. Rev.* B **43** 3423
[48] Kalugin P A 1992 *Phys. Rev.* B at press